iScience

CellPress
OPEN ACCESS

Article

CO_2 electroreduction favors carbon isotope ^{12}C over ^{13}C and facilitates isotope separation

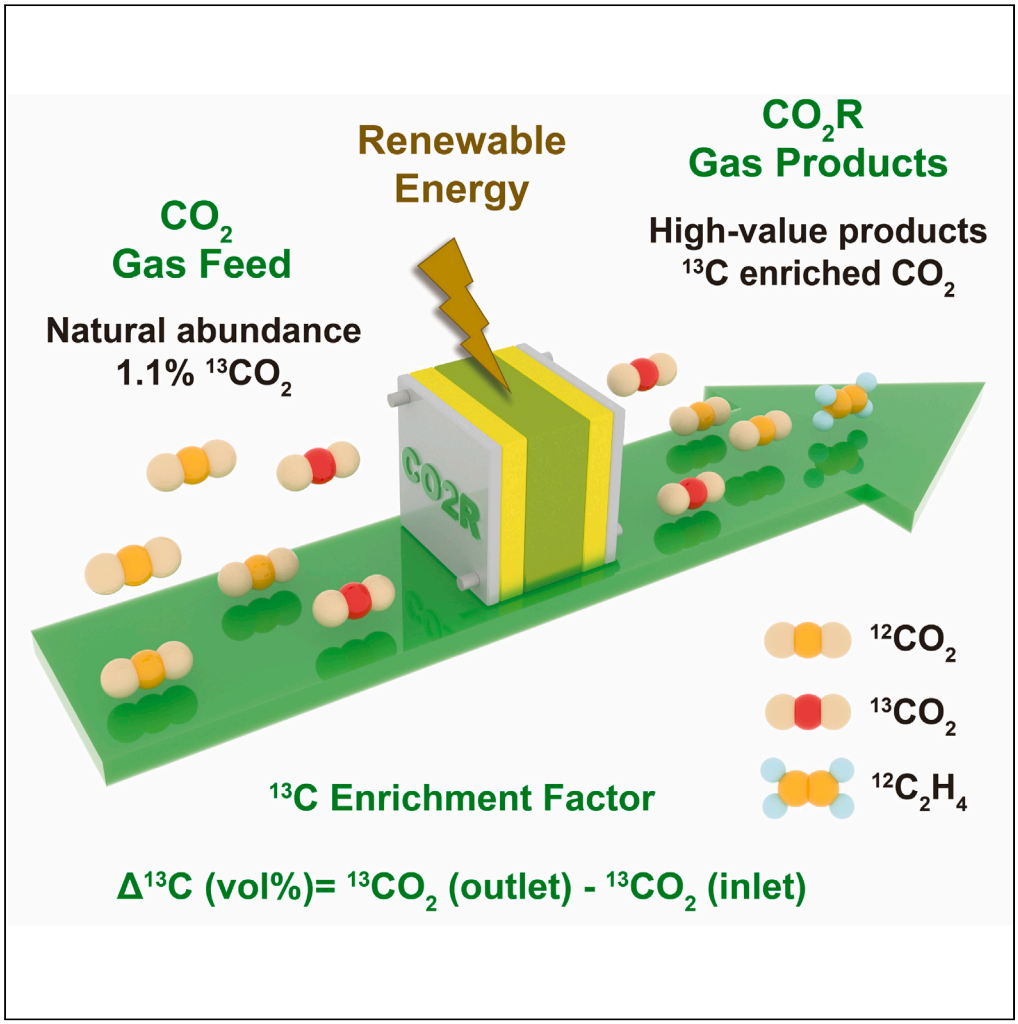

Magda H. Barecka, Mikhail K. Kovalev, Marsha Zakir Muhamad, Hangjuan Ren, Joel W. Ager, Alexei A. Lapkin

m.barecka@northeastern.edu

Highlights

CO_2 electroreduction strongly favors the conversion of ^{12}C isotope of carbon

Unreacted CO_2 is enriched in ^{13}C isotope – up to +18% after a single pass

We propose a scalable, economically viable process to separate carbon isotopes

We report a disruptive application of CO_2 electroreduction

Barecka et al., iScience *26*, 107834
October 20, 2023
https://doi.org/10.1016/j.isci.2023.107834

iScience

CellPress
OPEN ACCESS

Article

CO_2 electroreduction favors carbon isotope ^{12}C over ^{13}C and facilitates isotope separation

Magda H. Barecka,[1,2,3,9,*] Mikhail K. Kovalev,[3] Marsha Zakir Muhamad,[3] Hangjuan Ren,[3,4] Joel W. Ager,[5,6,7] and Alexei A. Lapkin[3,8]

SUMMARY

We discovered that CO_2 electroreduction strongly favors the conversion of the dominant isotope of carbon (^{12}C) and discriminates against the less abundant, stable carbon ^{13}C isotope. Both absorption of CO_2 in the alkaline electrolyte and CO_2 electrochemical reduction favor the lighter isotopologue. As a result, the stream of unreacted CO_2 leaving the electrolyzer has an increased ^{13}C content, and the depletion of ^{13}C in the product is several times greater than that of photosynthesis. Using a natural abundance feed, we demonstrate enriching of the ^{13}C fraction to ~1.3% (i.e., +18%) in a single-pass reactor and propose a scalable and economically attractive process to yield isotopes of a commercial purity. Our finding opens pathways to both cheaper and less energy-intensive production of stable isotopes (^{13}C, ^{15}N) essential to the healthcare and chemistry research, and to an economically viable, disruptive application of electrolysis technologies developed in the context of sustainability transition.

INTRODUCTION

By providing a unique opportunity to label chemically identical molecules, use of stable, benign isotopes has enabled breakthroughs in understanding of metabolic pathways,[1,2] drug discovery,[3] and in elucidating chemical transformations.[4] While there exist a wide range of applications for stable isotopes, their deployment is restricted by limited manufacturing capacities and the high costs of separation for rare isotopes.[5] Most separation techniques used in the chemical industry[6] exploit isotopic differences in physical properties such as, e.g., boiling point or effusion rate. Isotopes have very similar physical properties,[7] and the resulting separation processes are complex. Hence, industrial separation of isotopes requires hundreds of stages to achieve the desired isotopic purity, which leads to extended processing times, high energy consumption and costs,[8] and ultimately limits the supply of labeled compounds for healthcare and research. Consequently, the discovery of new methods that allow for a significant decrease in the price of isotope-enriched chemicals and its wider availability would be beneficial for science and technology.

Given the importance of improving the access to stable isotope materials, we sought to understand if rapidly evolving technologies developed in the context of energy transition (e.g., CO_2 electrolysis) could be adopted to separate isotopes. If successful, such methods could not only facilitate the access to isotopes but also foster the scale-up and deployment of carbon-neutral production of chemicals and fuels by providing an opportunity to deliver a high-value product. We focused on carbon-13 (^{13}C), a stable isotope of carbon with natural abundance of 1.1%, which is widely used in health sector[9] and recently also in the context of COVID treatment research and diagnosis,[10] contributing to a projected compound annual growth rate of 2.2% between 2020 and 2027.[11] ^{13}C-enriched compounds are non-radioactive (as opposed to ^{14}C), thus are safe[12] and can be used in protein quantification studies,[13] metabolic processes analysis (e.g., cancer metabolism[14]), and in medical diagnostic tests such as urea breath test for detection of the presence of *Helicobacter pylori* infection.[15]

Currently, ^{13}C is produced on industrial scale by cryogenic distillation of carbon monoxide or methane.[16] Because of the low natural abundance of ^{13}C in the feedstock materials, and difficulties to separate ^{12}C and ^{13}C, the existing ^{13}C production plants deploy over 100-meter-tall[17] columns to deliver the output of less than a ton per year (the largest reported ^{13}C manufacturing facility has a capability of ~525 kg of ^{13}C annually[18]). Based on reports from the industrially deployed process,[19] we estimate that it takes 15 days to pre-concentrate the CO stream from 1.1% to 10% ^{13}C content.

[1]Department of Chemical Engineering, Northeastern University, 360 Huntington Avenue, Boston, MA 02215, USA
[2]Department of Chemistry and Chemical Biology, Northeastern University, 360 Huntington Avenue, Boston, MA 02215, USA
[3]Cambridge Centre for Advanced Research and Education in Singapore, CARES Ltd. 1 CREATE Way, CREATE Tower #05-05, Singapore 138602, Singapore
[4]Department of Chemistry, University of Oxford, Oxford OX1 3QR, UK
[5]Berkeley Educational Alliance for Research in Singapore (BEARS), Ltd, 1 CREATE Way, Singapore 138602, Singapore
[6]Department of Materials Science and Engineering, University of California at Berkeley, Berkeley, CA 94720, USA
[7]Materials Sciences Division, Lawrence Berkeley National Laboratory, Berkeley, CA 94720, USA
[8]Department of Chemical Engineering and Biotechnology, University of Cambridge, Cambridge CB3 0AS, UK
[9]Lead contact
*Correspondence: m.barecka@northeastern.edu
https://doi.org/10.1016/j.isci.2023.107834

Consequently, there is significant interest in finding more scalable and cost-effective methods for separation of this important isotope. Thermal diffusion,[20,21] chemical exchange,[22] and reactive separation[23]-based methods were reported; however, none of these enhanced process efficiency enough to be able to penetrate the market. Laser separation,[24] an emerging commercial method for uranium and silicon separation, has also been studied for ^{13}C enrichment; however, their deployment necessitates the use of halogenated compounds such as e.g., $CHClF_2/Br_2$, and together with limited process efficiency, did not ultimately yield a feasible large-scale method.[25] Therefore, the need remains for an alternative isotope enrichment approach which will offer significant improvement in both economic and environmental dimensions.

Seeking for an alternative approach for ^{13}C production, we analyzed first the ^{13}C enrichment effect in photosynthesis. Within the naturally occurring carbon cycle, $^{12}CO_2$ isotopologue is preferentially used in the photosynthesis processes through several sub-steps (CO_2 absorption, conversion to photosynthesis precursors).[26] Consequently, ^{12}C is preferentially accumulated in biomass relative to ^{13}C.[27–29] We hypothesized that as CO_2 electrolysis (CO2R) has some similarities with photosynthesis, it might also discriminate ^{13}C over ^{12}C during the conversion of CO_2 to products containing one or more molecules of carbon. Furthermore, electrolysis, on its own, has been reported to manifest enrichment effect for the case of lithium isotopes separation.[30,31] Even though this effect is minor, we anticipated that by careful control of all molecular events happening in CO_2 electrolysis, we might be able to further intensify the electrochemistry-related enrichment and, ultimately, use CO_2 electroreduction as an efficient method to produce ^{13}C isotope.

RESULTS

To investigate our hypothesis, we performed a series of CO2R experiments, using gas-diffusion electrode (GDE)-based flow cells, with gaseous CO_2 supplied on the cathode side and potassium hydroxide solutions used as catholyte and anolyte (Figure 1A; electrodes characterization is given in Figures S1 and S2; single-pass CO_2 utilization is tracked in Table S2 (inlet vs. outlet CO_2 stream)). $^{12}CO_2$ undergoes chemical reactions faster than $^{13}CO_2$, following the general principle of a lower activation energy for lighter isotopologues in irreversible reactions.[32–35] Heavier isotopes are associated with lower zero-point energy. As a result, more energy is needed to break their bonds, resulting in a higher activation energy for the heavier isotopologues.[35] We expected that the unreacted CO_2 leaving the reactor will be enriched in ^{13}C isotope; therefore, we sought to simulate a variety of conditions that will lead to different rates of CO_2 conversion at GDEs favoring different products (C1 or C2). We deployed varied flow rates of CO_2 (30–75 sccm), current densities (0.5–1 A/cm^2), different GDEs (Ag and Cu), and used quadrupole mass analyzer (QMS) to quantify ^{13}C content in the unreacted CO_2 stream by recording $^{12}CO_2$ and $^{13}CO_2$ for 44 and 45 *m/z* peaks counts, respectively. Mass spectrometry is frequently used for precise quantification of stable ^{13}C abundance, and most importantly, allows for real-time analysis.[36] We sought to quantify delta ^{13}C defined as the difference between $^{13}CO_2$ concentration (mol %) at the reactor outlet and inlet (using natural abundance CO_2 feed with 1.1% of ^{13}C isotope) (Equation 1).

$$\Delta^{13}C = {}^{13}CO_2\ conc.\ outlet - {}^{13}CO_2\ conc.\ inlet \quad \text{(Equation 1)}$$

Across all experiments on Ag and Cu (Figures 1B and 1C) GDEs, we observed a notable ^{13}C enrichment effect, which increased with current, allowing to achieve $\Delta^{13}C$ of up to ~0.15%, yielding CO_2 stream with 1.25% ^{13}C content. This exceptionally high (compared to the previously reported separation methods) concentration achieved after a single pass through a GDE reactor was observed on a silver GDE under the conditions which favor high CO_2 conversion (1 A/cm^2, 30 sccm of CO_2 inlet flow rate); the Cu GDE allowed to achieve much lower $\Delta^{13}C$.

There are two highly intriguing aspects of these phenomena. First, the enrichment is achieved almost immediately, as opposed to the industrially deployed method that needs hours to days processing time to achieve the same enrichment rate. Secondly, the enrichment effect is observed for different starting concentrations of ^{13}C. We performed an experiment on the Ag GDE stream containing 5% of ^{13}C CO_2 and observed the same level of isotope enrichment, suggesting that the discovered phenomenon could be observed while running a multi-stage electrolysis, where the outlet gas from one stage is fed to another. Thus, on the fundamental level, the phenomena could be scaled to obtain even a >5% pure $^{13}CO_2$ (Figure S3).

To confirm our findings, we used two other methods for isotope fractionation measurements: proton-transfer reaction time-of-flight mass spectrometry (PTR-TOF-MS)[37,38] and Fourier transform infrared spectroscopy (FTIR) (methods details and raw data are available in Supplementary Text). Our experimental setup (Figure S4) involved simultaneous measurement of ^{13}C content by both methods by deploying a split of the gas sample leaving the reactor to PTR-TOF-MS and FTIR. Not only did we find a perfect agreement between all measurement methods (Figure S5) but we also explored the effect of further increasing the current up to 1.5 A/cm^2, reaching the enrichment effect of $\Delta^{13}C$ of 0.20% on a silver electrode +/− 0.04% (Figures 1C and 1D).

Seeking to understand the mechanism driving the significant isotopic effect, we deployed gas chromatography to separate and precisely quantify[39] gaseous reaction products (ethylene, carbon monoxide, hydrogen) and NMR for liquid products (e.g., ethanol). We expected that the isotope enrichment effect is primarily observed due to CO_2 reduction reactions, thus increased Faradaic efficiency to carbon-containing products should be associated with higher delta ^{13}C. In contrast to what was expected, high Faradaic efficiency for products such as carbon monoxide on Ag GDE (Figure 1F) and ethylene on Cu GDE (Figure 1H) did not correlate with high ^{13}C enrichment. Therefore, we hypothesized a correlation of the isotope enrichment with decreasing concentration of CO_2 remaining in the stream (Figures 1G and 1I). We first sought to explain this based on the conversion to carbon reduced products, since it is visibly higher on Ag than on Cu (Figures 1G and 1I), correlating with higher enrichment. However, analyzing the product distribution for the Ag cathode, we noted the fraction of carbon monoxide in the outlet gas for the 1A and 1.5A experiments are not significantly different (Figure 1G); what does increase is the concentration of hydrogen.

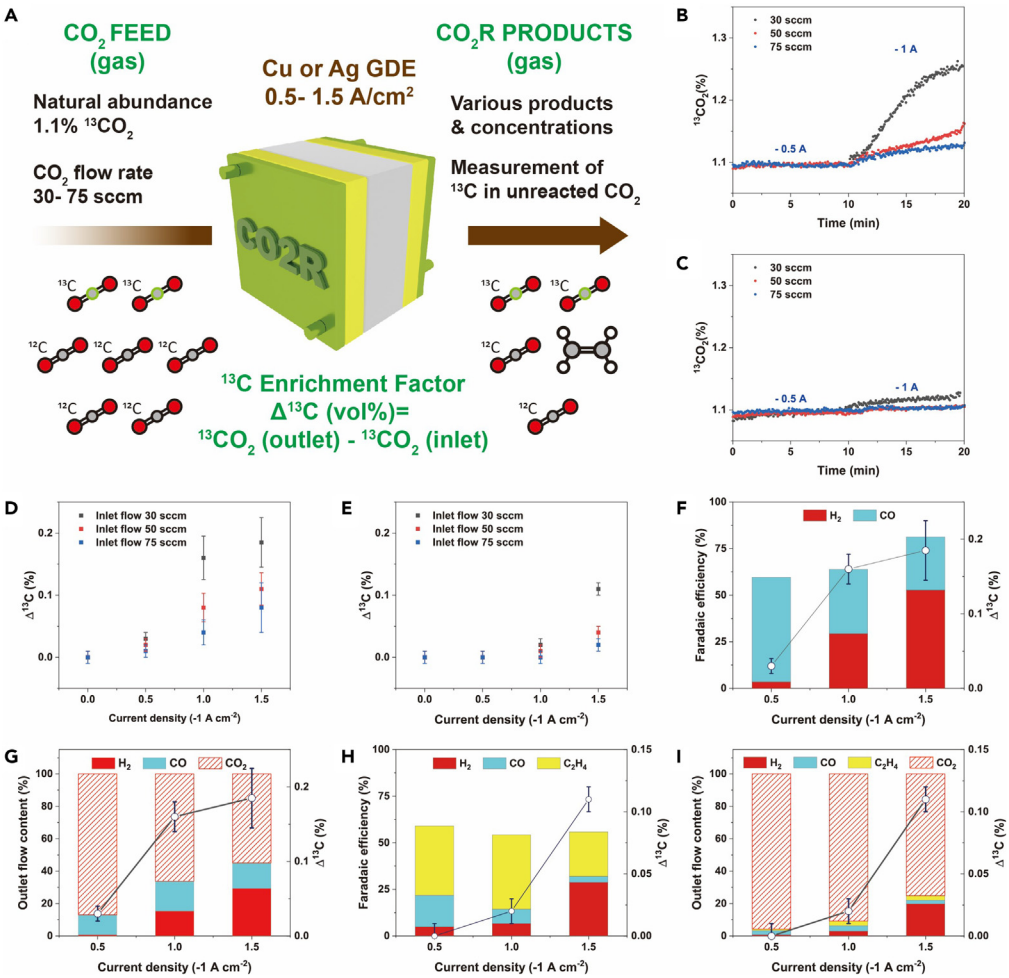

Figure 1. ^{13}C enrichment effect during high current CO2R on Ag and Cu GDEs

(A–E) (A) A schematic representation of the experimental setup used; (B) QMS raw data for ^{13}C enrichment on a silver and (C) copper GDEs, the effect has a slight delay because of saturation time needed for QMS ionization chamber; (D) ^{13}C enrichment observed at the outlet of the flow reactor for different flow rates and current densities on silver and (E) copper GDEs.

(F–I) (F) Faradaic efficiencies (FE) of CO_2 electroreduction for main products at different current densities at 30 sccm inlet flow on Ag GDE; (G) Outlet flow composition (mol %) for Ag GDE, 30 sccm CO_2 inlet flow; (H) FE for main products for Cu GDE, 30 sccm CO_2 inlet flow; (I) Outlet flow content for Cu GDE 30 sccm CO_2 inlet flow. All experiments were performed using 3.5 M KOH as catholyte. All data are reported in Tables S2 and S3. The standard error bars were set as 95% confidence interval.

We therefore investigated whether CO_2 electroreduction is indeed the only mechanism contributing to the observed enrichment and scrutinized the potential isotope discrimination in chemical CO_2 capture happening at the gas-catholyte interface. The isotope effects related to the intake of CO_2 in basic solutions have been thoroughly studied in the field of oceanography.[40,41] The rate of ^{13}C intake into oceans is used to track the global carbon cycle and it is well known that absorption of CO_2 in basic media manifests a minor isotopic effect, leading to preferential capture of ^{12}C isotope.[42] However, as the discrimination effect in ocean waters is minor, it has never been explored in industrial applications. To quantify the contribution of the absorption step, we performed experiments without applying a potential to the working electrode and as anticipated, observed a minimal ^{13}C enrichment effect ($\Delta^{13}C$–0.02 in 3.5 M KOH solution) (Figure S6), which on its own, is unlikely to meaningfully contribute to the observed isotope discrimination phenomena under the electroreduction conditions.

There is, however, another phenomenon that we must consider. The rate of chemical CO_2 capture is significantly intensified at an electrochemical interface. Reported by Ma et al.,[43] CO_2 pumping occurs during electrolysis in basic media, where proton consumption leads to hydroxide generation, which reacts with CO_2 to form bicarbonate, resulting in CO_2 capture (Equations 2 and 3). Subsequently, carbonate/bicarbonate ions diffuse through the membrane separating the catholyte and anolyte chambers, and CO_2 degasses on the anode side (Equations 4 and 5). This significantly limits the maximum efficiency of the electrolyzer and, thus, imposes a hurdle toward commercialization of electrolysis.[44] We hence sought to understand how CO_2 pumping contributes to isotope balancing and performed experiments using a catalyst-free carbon paper instead of Ag or Cu GDEs.

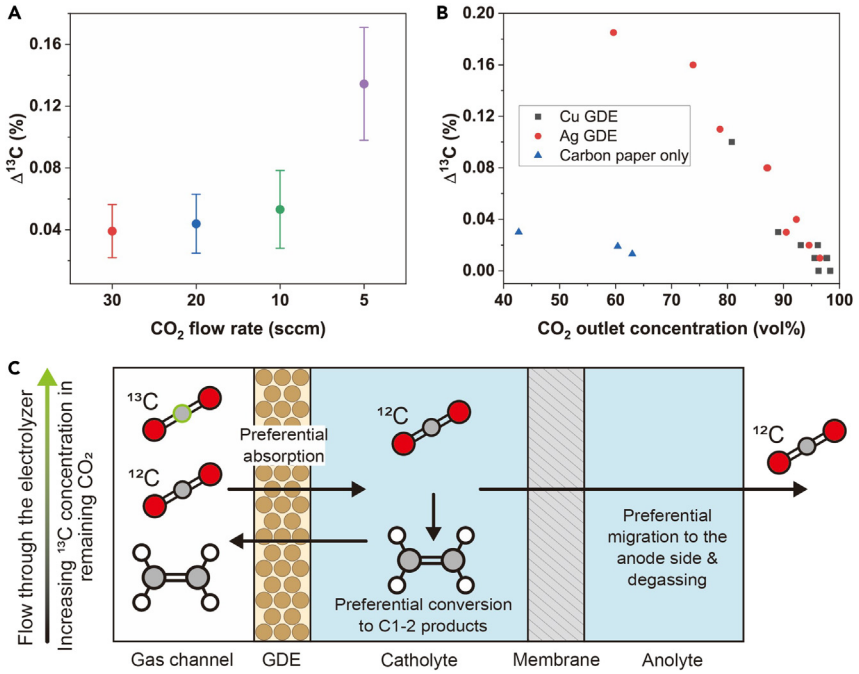

Figure 2. Investigation of CO_2 pumping effects in ^{13}C enrichment via CO2R

(A–C) (A) $\Delta^{13}C$ measured during electrolysis experiments performed using carbon paper instead of Ag or Cu GDEs, catholyte used: 3.5 M KOH; (B) the attained ^{13}C enrichment is a function of CO_2 concentration at the electrolyzer outlet; (C) depiction of the suggested reactive separation mechanisms, where ^{12}C is being preferentially consumed in a cascade of phenomena happening inside of CO_2 electrolyzer and thus ^{13}C enriches in the unreacted gas.

In the absence of CO_2 electroreduction catalyst, no CO2R was observed, allowing us to quantify the sole effect of CO_2 pumping. Intriguingly, at the lowest CO_2 flow rate used in previous experiments, we observed meaningful ^{13}C enrichment effect and were able to intensify it up to $\Delta^{13}C$ of 0.13% (Figure 2A).

$$OH^- + CO_2 \leftrightarrow HCO_3^- \quad \text{(Equation 2)}$$

$$OH^- + HCO_3^- \leftrightarrow CO_3^{2-} + H_2O \quad \text{(Equation 3)}$$

$$HCO_3^- + H^+ \rightarrow CO_2 + H_2O \quad \text{(Equation 4)}$$

$$CO_3^{2-} + 2H^+ \rightarrow CO_2 + H_2O \quad \text{(Equation 5)}$$

DISCUSSION

Looking at the summary of all our experiments (Figure 2B), there is an apparent relationship between ^{13}C enrichment and the remaining CO_2 concentration, suggesting that all steps involved in the CO_2 electroreduction reactors (absorption, reaction, degassing) contribute to the enrichment mechanism. The rate of enrichment is significantly higher when CO2R electrocatalysts are used (correlation of the left side of Figure 2B) and is slower in the absence of CO_2 conversion step (right side of Figure 2B). The observation of $\Delta^{13}C$ on carbon paper without catalysts suggests that the generation of products that do not contain carbon—such as hydrogen—also contributes to the enrichment effect, which can be explained based on CO_2 pumping mechanism. As a result of hydrogen formation, more OH^- ions are being present at the cathode surface, and thus, facilitate capture of CO_2 into HCO_3^- and subsequently CO_3^{2-} ions, which manifests minor isotope discrimination effect. While CO_2 absorption into the electrolyte, on its own, would yield an almost negligible ^{13}C enrichment, coupling it at the same space and time with removal mechanisms (CO_2 conversion into electrolysis products and carbonate/bicarbonate ions migration and degassing) enables to vacate more space for selective ^{12}C intake, preferred over ^{13}C as the lighter isotope.[35] This, in turn, enriches ^{13}C content in the outlet stream based on reactive absorption mechanism (Figure 2C). Thus, the enrichment is not strongly dependent on the type of product formed, but rather on the intensity of the cascade of isotope-sensitive phenomena happening inside the electrolyzer.

Looking toward practical applications of scaled-up isotope production by CO2R, we sought to conceptually design the entire process and perform a techno-economic analysis. We first verified if ^{13}C enrichment effect could be maintained during an extended period of time and demonstrated 5 h of stable enrichment, at a current density of 1 A cm^{-2}, five times higher than typically deployed in long-term runs for electrolysis on Ag GDEs[45,46] (Figure 3A). Further, we screened the potential applications for ^{13}C-enriched stream and noted that there are many processes

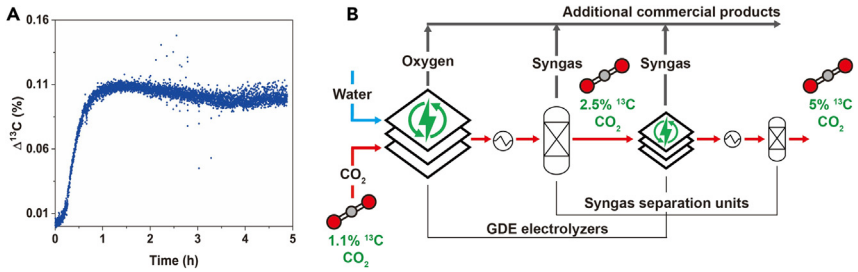

Figure 3. Scale-up considerations of CO2R-based ^{13}C isotope enrichment method

(A and B) (A) A stability test performed on Ag GDE, under 1 A/cm^2 current density and 50 sccm feed CO_2 flow rate, note that cell run at 0 A for the first 15 min, then 20 min at −0.5 A, and the rest at −1.5 A; (B) a concept of a process of electrolysis-based production of 5% ^{13}C-enriched CO_2 stream. The process deploys 9 consecutive electrolyzers allowing to achieve ∼5% concentration of CO_2 at outlet of the last reactor; each subsequent electrolyzer has a reduced size as required for conversion of a lower CO_2 stream remaining unreacted after the first electrolysis step.

that do not necessarily require high ^{13}C content. A ^{13}C-enriched CO_2 stream is widely deployable as a starting material for synthesis of labeled compounds, with 5% ^{13}C being used in isotope ratio outlier analysis for tracking metabolites,[47] and 10% ^{13}C-enriched CO_2 cylinders being a commodity product.[48] We conceptualized the electrolysis-based process, capable of delivering 5% ^{13}C feed (Figure 3B, modeling details in supplemental information, Process Modelling). The proposed process is based on deployment of Ag GDE which is also reported as being more stable and has a higher technology readiness level.[45] Extrapolating from the experimentally obtained relationship between CO_2 concentration at the outlet and the ^{13}C enrichment for Ag GDE, we assessed that it could be possible to achieve 1.5% ^{13}C content at the outlet of a single reactor, at 50% CO_2 conversion, being a feasible target in the context of recent reports on electrolysis scale-up.[49,50] Hence, a series of 9 electrolyzers would suffice to yield the target 5% enrichment. The stream of gas leaving each of the reactors will contain a ^{13}C-enriched CO_2 stream, as well as a significant amount of hydrogen and carbon monoxide. CO_2 can be separated from this mixture by means of e.g., solution-diffusion based membranes[51] or low-temperature separation[52] deployed for industrial purification of syngas, yielding pure ^{13}C-enriched CO_2 stream.

To quantify the techno-economic performance of the process including electrolyzers and the necessary separation steps, we used a recently reported protocol designed for the evaluation of emerging electrolysis technologies.[53] Since CO_2 electrolysis is still early-development stages, we assumed high-price indicators (0.05 $/kWh of renewable energy powering the process,[54] 200 $/t of CO_2, as reported for air-based CO_2 capture[55]) to account for the potential limitations in the energy efficiency and avoid overestimation of the economic viability. We assessed the cost of manufacturing of 5% ^{13}C-enriched stream as ∼0.8 $/L, which represents a drastic cost reduction (the cost of commercially ^{13}C-enriched stream is assessed ∼16 $/L; SI, Techno-economic analysis and Table S6). While the current process knowledge is too scarce to accurately assess the life cycle environmental footprint of our method, we anticipate that the proposed alternative offers improvements in terms of decarbonization of isotopes production. Electrolysis necessitates only the input of electric energy, which can be sourced from renewables sector, and instead of petrochemical feedstocks, uses CO_2 as a feed, obtainable from biogenic sources or ambient air. Importantly, electrolysis is a modular technology; therefore, it is straightforward to scale and deploy close to the final user, further simplifying access to stable isotopes. Our method reduces significantly the time needed to process ^{13}C-enriched streams, from days-long distillation campaigns to a range of minutes necessary for CO_2 electrolysis and separation.

Importantly, based on our experiment where we used a 5% ^{13}C CO_2 feed and still observed significant isotope enrichment, the electrolysis-based technology could be also used to obtain streams of highly pure $^{13}CO_2$; however, this would require a higher number of reactor and separation steps in between.

In summary, we have identified a significant potential for CO_2 electroreduction to broaden access to sustainable ^{13}C-labeled compounds. More generally, the electrochemical enrichment mechanism opens pathways to more selective and sustainable separation of the compounds exhibiting very similar physical properties, which can be explored across the entire market for isotopes production.

Notably, the further development of proposed isotopes enrichment technology will also contribute to the growth of CO_2 electrolysis as a method to produce chemical building blocks and fuels. Because of the low prices of petrochemically derived hydrocarbon molecules, it is currently challenging to showcase a competitive production method by means of CO2R. On the contrary, the excellent economic case of electrolysis-based isotopes production can motivate investment into CO2R scale-up, which will ultimately lead to the improvement of the reactor mass and energy efficiency, stability, and decrease the investment cost, necessary to penetrate chemicals and fuels production markets. Our discovery opens a new pathway for deployment of CO_2 electrolysis. The benefits of such a synergistic development effort would span across healthcare, research, and chemical sectors, and in a long term, be an important steppingstone in the pursuit of Net Zero 2050 goal.

Limitations of the study

Future research will require precise characterization of the isotope discrimination effect for each reaction and each molecule produced by CO2R. Recent work by Ren et al.[56] demonstrated indeed that some of the liquid products of CO2R (e.g.,) have a higher ratio of ^{12}C/^{13}C than the natural abundance (since the lighter isotope reacts more easily). However, to mathematically represent suggested complex mechanism, measurements of ^{12}C/^{13}C ratios will be required not only for all products but also on different interfaces present in the electrochemical reactors.

While we deployed independent measurements methods (QMS and FTIR) to confirm the outstandingly high isotope enrichment effect, it is worthy to note that we observed the highest $^{13}CO_2$ concentration under the conditions of higher hydrogen content in the mixture. While based on the working principle of QMS and FTIR, this should not affect the measurement accuracy; future measurements should be ideally performed with pure CO_2 gas.

STAR★METHODS

Detailed methods are provided in the online version of this paper and include the following:

- KEY RESOURCES TABLE
- RESOURCE AVAILABILITY
  - Lead contact
  - Materials availability
  - Data and code availability
- METHOD DETAILS
  - Synthesis materials
  - Copper nanoparticles synthesis
  - Copper gas diffusion electrode fabrication
  - Silver gas diffusion electrode fabrication
  - NiFe-OOH anode fabrication (electrodeposition)
  - CO2R flow cell and electrochemical measurements
  - Analytical methods: Gas chromatography
  - NMR
  - Mass spectrometry
  - PTR-TOF-MS
  - PTR-TOF-MS background signal estimation
  - FTIR
  - Flow cell characterization and products
  - Faradaic efficiency calculations
  - Process modelling
  - Techno-economic analysis

SUPPLEMENTAL INFORMATION

Supplemental information can be found online at https://doi.org/10.1016/j.isci.2023.107834.

ACKNOWLEDGMENTS

This work was supported by the National Research Foundation (NRF), Prime Minister's Office, Singapore under its Campus for Research Excellence and Technological Enterprise (CREATE) Program through the eCO2EP project operated by the Cambridge Centre for Advanced Research and Education in Singapore (CARES) and the Berkeley Educational Alliance for Research in Singapore (BEARS). The contribution of Andres J. Sanz Guillen to the enrichment of the visual content is gratefully acknowledged.

AUTHOR CONTRIBUTIONS

Initial phenomena observation, M.K.K., M.H.B; investigation, GDE fabrication, and cell setup, M.Z.M., H.R., and M.K.K.; EC measurements, M.Z.M.; PTRMS, M.K.K.; QMS, M.Z.M., M.K.K., and M.H.B.; methodology, M.H.B., M.K.K., and J.W.A.; data curation, M.K.K., M.H.B., and J.W.A.; formal analysis, M.H.B., M.K.K., and J.W.A.; TEA and process model, M.H.B.; visualization, M.K.K., M.H.B., M.Z.M., and J.W.A.; writing – original draft, M.H.B., M.Z.M., M.K., and J.W.A.; review and editing, all. Supervision, project administration, and funding acquisition, J.W.A. and A.A.L.

DECLARATION OF INTERESTS

The authors filed non-provisional patent application PCT/SG2022/050430 covering the electrochemical process for enrichment of stable carbon-13 isotope.

Received: April 12, 2023
Revised: July 24, 2023
Accepted: September 1, 2023
Published: September 26, 2023

REFERENCES

1. Schoenheimer, R., and Rittenberg, D. (1935). Deuterium as an Indicator in the Study of Intermediary Metabolism. Science *82*, 156–157. https://doi.org/10.1126/science.82.2120.156.
2. Lacroix, M., Mosora, F., Pontus, M., Lefebvre, P., Luyckz, A., and Lopez-Habib, G. (1973). Glucose Naturally Labeled with Carbon-13: Use for Metabolic Studies in Man. Science *181*, 445–446. https://doi.org/10.1126/science.181.4098.445.
3. Elmore, C.S., and Bragg, R.A. (2015). Isotope chemistry; a useful tool in the drug discovery arsenal. Bioorg. Med. Chem. Lett. *25*, 167–171. https://doi.org/10.1016/j.bmcl.2014.11.051.
4. Andersen, S.Z., Čolić, V., Yang, S., Schwalbe, J.A., Nielander, A.C., McEnaney, J.M., Enemark-Rasmussen, K., Baker, J.G., Singh, A.R., Rohr, B.A., et al. (2019). A rigorous electrochemical ammonia synthesis protocol with quantitative isotope measurements. Nature *570*, 504–508. https://doi.org/10.1038/s41586-019-1260-x.
5. Ledovskaya, M.S., Voronin, V.V., Rodygin, K.S., and Ananikov, V.P. (2020). Efficient labeling of organic molecules using ^{13}C elemental carbon: universal access to $^{13}C_2$-labeled synthetic building blocks, polymers and pharmaceuticals. Org. Chem. Front. *7*, 638–647. https://doi.org/10.1039/C9QO01357A.
6. Henley, E., Seader, J.D., and Roper, K. (2012). Separation Process Principles, 3rd Edition (Wiley).
7. R. Michener, and K. Lajtha, eds. (2007). Stable Isotopes in Ecology and Environmental Science (Blackwell Publishing Ltd). https://doi.org/10.1002/9780470691854.
8. Johns, T.F. (2013). Isotope separation by multistage methods. In Progress in Nuclear Physics (Elsevier), pp. 1–25. https://doi.org/10.1016/B978-1-4831-9887-3.50005-0.
9. Bütz, D.E., Casperson, S.L., and Whigham, L.D. (2014). The emerging role of carbon isotope ratio determination in health research and medical diagnostics. J. Anal. At. Spectrom. *29*, 594–598. https://doi.org/10.1039/C3JA50327E.
10. DataM Intelligence (2021). Stable Isotope Labeled Compound Market. Market report by DataM Intelligence SKU: DM3071, extract. https://www.datamintelligence.com/research-report/stable-isotope-labeled-compound-market2021.
11. Newswire, G. (2021). Global Stable Isotope Labeled Compounds Industry. https://www.globenewswire.com/news-release/2020/07/30/2069966/0/en/Global-Stable-Isotope-Labeled-Compounds-Industry.html.
12. Koletzko, B., Sauerwald, T., and Demmelmair, H. (1997). Safety of stable isotope use. Eur. J. Pediatr. *156*, S12–S17. https://doi.org/10.1007/PL00014267.
13. Allen, D.K., Goldford, J., Gierse, J.K., Mandy, D., Diepenbrock, C., and Libourel, I.G.L. (2014). Quantification of Peptide *m/z* Distributions from ^{13}C-Labeled Cultures with High-Resolution Mass Spectrometry. Anal. Chem. *86*, 1894–1901. https://doi.org/10.1021/ac403985w.
14. Antoniewicz, M.R. (2018). A guide to 13C metabolic flux analysis for the cancer biologist. Exp. Mol. Med. *50*, 1–13. https://doi.org/10.1038/s12276-018-0060-y.
15. Abd Rahim, M.A., Johani, F.H., Shah, S.A., Hassan, M.R., and Abdul Manaf, M.R. (2019). ^{13}C-Urea Breath Test Accuracy for *Helicobacter pylori* Infection in the Asian Population: A Meta-Analysis. Ann. Glob. Health *85*, 110. https://doi.org/10.5334/aogh.2570.
16. Pellegrini, L.A., Sangiorgio, V.A., De Guido, G., Szücs-Balazs, J.Z., and Gligan, M.L. (2020). Optimization of 13C enrichment by carbon monoxide cryogenic distillation. Chem. Eng. Res. Des. *160*, 499–507. https://doi.org/10.1016/j.cherd.2020.06.010.
17. McInteer, B.B. (1980). Isotope Separation by Distillation: Design of a Carbon-13 Plant. Separ. Sci. Technol. *15*, 491–508. https://doi.org/10.1080/01496398008068494.
18. Cambridge Isotope Laboratories (2021). Corporate Overview. Retrived 3/11/2021. https://www.isotope.com/corporate-overview/history.cfm.
19. Li, H.-L., Ju, Y.-L., Li, L.-J., and Xu, D.-G. (2010). Separation of isotope 13C using high-performance structured packing. Chem. Eng. Process: Process Intensif. *49*, 255–261. https://doi.org/10.1016/j.cep.2010.02.001.
20. Watson, W.W. (1941). Heavy Carbon Production by Thermal Diffusion. Science *93*, 473–474. https://doi.org/10.1126/science.93.2420.473.
21. Nier, A.O., and Bardeen, J. (1941). The Production of Concentrated Carbon (13) by Thermal Diffusion. J. Chem. Phys. *9*, 690–692. https://doi.org/10.1063/1.1750978.
22. Ghate, M.R., and Taylor, T.I. (1975). Production of ^{13}C by Chemical Exchange Reaction between Amine Carbamate and Carbon Dioxide in a Solvent-Carrier System. Separ. Sci. *10*, 547–569. https://doi.org/10.1080/00372367508058040.
23. Bernstein, R.B. (1957). Simple Laboratory Method for Producing Enriched Carbon-13. Science *126*, 119–120. https://doi.org/10.1126/science.126.3264.119.
24. SILEX (2023). SILEX. SILEX Laser Separation Technology (Company website). https://www.silex.com.au/silex-technology/silex-laser-isotope-separation-technology/2021.
25. Gauthier, M., Cureton, C.G., Hackett, P.A., and Willis, C. (1982). Efficient production of13C2F4 in the infrared laser photolysis of CHClF2. Appl. Phys. B *28*, 43–50. https://doi.org/10.1007/BF00693891.
26. Tcherkez, G., Mahé, A., and Hodges, M. (2011). 12C/13C fractionations in plant primary metabolism. Trends Plant Sci. *16*, 499–506. https://doi.org/10.1016/j.tplants.2011.05.010.
27. Werner, C., Schnyder, H., Cuntz, M., Keitel, C., Zeeman, M.J., Dawson, T.E., Badeck, F.-W., Brugnoli, E., Ghashghaie, J., Grams, T.E.E., et al. (2012). Progress and challenges in using stable isotopes to trace plant carbon and water relations across scales. Biogeosciences *9*, 3083–3111. https://doi.org/10.5194/bg-9-3083-2012.
28. Farquhar, G.D., Ehleringer, J.R., and Hubick, K.T. (1989). Carbon Isotope Discrimination and Photosynthesis. Annu. Rev. Plant Physiol. Plant Mol. Biol. *40*, 503–537. https://doi.org/10.1146/annurev.pp.40.060189.002443.
29. Diefendorf, A.F., Mueller, K.E., Wing, S.L., Koch, P.L., and Freeman, K.H. (2010). Global patterns in leaf ^{13}C discrimination and implications for studies of past and future climate. Proc. Natl. Acad. Sci. USA *107*, 5738–5743. https://doi.org/10.1073/pnas.0910513107.
30. Black, J.R., Umeda, G., Dunn, B., McDonough, W.F., and Kavner, A. (2009). Electrochemical Isotope Effect and Lithium Isotope Separation. J. Am. Chem. Soc. *131*, 9904–9905. https://doi.org/10.1021/ja903926x.
31. Acosta, L.N., and Flexer, V. (2018). A First Assessment on the Scale-Up Possibilities of Different Electrochemical Techniques for Lithium Isotopic Enrichment. Ind. Eng. Chem. Res. *57*, 11399–11413. https://doi.org/10.1021/acs.iecr.8b01640.
32. Dale, H.J.A., Leach, A.G., and Lloyd-Jones, G.C. (2021). Heavy-Atom Kinetic Isotope Effects: Primary Interest or Zero Point? J. Am. Chem. Soc. *143*, 21079–21099. https://doi.org/10.1021/jacs.1c07351.
33. Atkins, P.W., and De Paula, J. (2006). Atkins' Physical Chemistry, 8th ed. (Oxford University Press).
34. Laidler, K.J. (1987). Chemical Kinetics, 3rd ed. (Harper & Row).
35. Roth, J.P., and Klinman, J.P. (2004). Kinetic Isotope Effects. In Encyclopedia of Biological Chemistry (Elsevier), pp. 522–527. https://doi.org/10.1016/B0-12-443710-9/00351-3.
36. Hunter, E.P.L., and Lias, S.G. (1998). Evaluated Gas Phase Basicities and Proton Affinities of Molecules: An Update. J. Phys. Chem. Ref. Data *27*, 413–656. https://doi.org/10.1063/1.556018.
37. Hansel, A., Jordan, A., Holzinger, R., Prazeller, P., Vogel, W., and Lindinger, W. (1995). Proton transfer reaction mass spectrometry: on-line trace gas analysis at the ppb level. Int. J. Mass Spectrom. Ion Process. *149–150*, 609–619. https://doi.org/10.1016/0168-1176(95)04294-U.
38. Jordan, A., Haidacher, S., Hanel, G., Hartungen, E., Herbig, J., Märk, L., Schottkowsky, R., Seehauser, H., Sulzer, P., and Märk, T. (2009). An online ultra-high sensitivity Proton-transfer-reaction mass-spectrometer combined with switchable reagent ion capability (PTR+SRI−MS). Int. J. Mass Spectrom. *286*, 32–38. https://doi.org/10.1016/j.ijms.2009.06.006.
39. Niu, Z.-Z., Chi, L.-P., Liu, R., Chen, Z., and Gao, M.-R. (2021). Rigorous assessment of CO_2 electroreduction products in a flow cell. Energy Environ. Sci. *14*, 4169–4176. https://doi.org/10.1039/D1EE01664D.
40. Zeebe, R.E., Wolf-Gladrow, D.A., and Jansen, H. (1999). On the time required to establish chemical and isotopic equilibrium in the carbon dioxide system in seawater. Mar. Chem. *65*, 135–153. https://doi.org/10.1016/S0304-4203(98)00092-9.
41. Mackensen, A., and Schmiedl, G. (2019). Stable carbon isotopes in paleoceanography: atmosphere, oceans, and sediments. Earth Sci. Rev. *197*, 102893. https://doi.org/10.1016/j.earscirev.2019.102893.
42. Wanninkhof, R. (1985). Kinetic fractionation of the carbon isotopes ^{13}C and ^{12}C during transfer of CO_2 from air to seawater. Tellus B *37*, 128. https://doi.org/10.3402/tellusb.v37i3.15008.
43. Ma, M., Clark, E.L., Therkildsen, K.T., Dalsgaard, S., Chorkendorff, I., and Seger, B. (2020). Insights into the carbon balance for CO_2 electroreduction on Cu using gas diffusion electrode reactor designs. Energy Environ. Sci. *13*, 977–985. https://doi.org/10.1039/D0EE00047G.
44. Rabinowitz, J.A., and Kanan, M.W. (2020). The future of low-temperature carbon dioxide

electrolysis depends on solving one basic problem. Nat. Commun. *11*, 5231. https://doi.org/10.1038/s41467-020-19135-8.

45. Kutz, R.B., Chen, Q., Yang, H., Sajjad, S.D., Liu, Z., and Masel, I.R. (2017). Sustainion Imidazolium-Functionalized Polymers for Carbon Dioxide Electrolysis. Energy Technol. *5*, 929–936. https://doi.org/10.1002/ente.201600636.
46. Haas, T., Krause, R., Weber, R., Demler, M., and Schmid, G. (2018). Technical photosynthesis involving CO2 electrolysis and fermentation. Nat. Catal. *1*, 32–39. https://doi.org/10.1038/s41929-017-0005-1.
47. Stupp, G.S., Clendinen, C.S., Ajredini, R., Szewc, M.A., Garrett, T., Menger, R.F., Yost, R.A., Beecher, C., and Edison, A.S. (2013). Isotopic Ratio Outlier Analysis Global Metabolomics of Caenorhabditis elegans. Anal. Chem. *85*, 11858–11865. https://doi.org/10.1021/ac4025413.
48. Aldrich, S. (2023). Carbon-13C dioxide 10% Safety Data Sheet. https://www.sigmaaldrich.com/SG/en/sds/aldrich/600180.
49. Garg, S., Li, M., Weber, A.Z., Ge, L., Li, L., Rudolph, V., Wang, G., and Rufford, T.E. (2020). Advances and challenges in electrochemical CO_2 reduction processes: an engineering and design perspective looking beyond new catalyst materials. J. Mater. Chem. A *8*, 1511–1544. https://doi.org/10.1039/C9TA13298H.
50. Barecka, M.H., Ager, J.W., and Lapkin, A.A. (2021). Carbon neutral manufacturing via on-site CO2 recycling. iScience *24*, 102514. https://doi.org/10.1016/j.isci.2021.102514.
51. Poudel, J., Choi, J., and Oh, S. (2019). Process Design Characteristics of Syngas (CO/H2) Separation Using Composite Membrane. Sustainability *11*, 703. https://doi.org/10.3390/su11030703.
52. Berstad, D., Nekså, P., and Gjøvåg, G.A. (2011). Low-temperature syngas separation and CO2 capture for enhanced efficiency of IGCC power plants. Energy Proc. *4*, 1260–1267. https://doi.org/10.1016/j.egypro.2011.01.182.
53. Barecka, M.H., Ager, J.W., and Lapkin, A.A. (2021). Techno-economic assessment of emerging CO2 electrolysis technologies. STAR Protoc. *2*, 100889. https://doi.org/10.1016/j.xpro.2021.100889.
54. International Energy Agency (2020). Levelised Cost of Electricity Calculator. https://www.iea.org/data-and-statistics/data-tools/levelised-cost-of-electricity-calculator.
55. Sabatino, F., Grimm, A., Gallucci, F., van Sint Annaland, M., Kramer, G.J., and Gazzani, M. (2021). A comparative energy and costs assessment and optimization for direct air capture technologies. Joule *5*, 2047–2076. https://doi.org/10.1016/j.joule.2021.05.023.
56. Ren, H., Kovalev, M., Weng, Z., Muhamad, M.Z., Ma, H., Sheng, Y., Sun, L., Wang, J., Rihm, S., Yang, W., et al. (2022). Operando proton-transfer-reaction time-of-flight mass spectrometry of carbon dioxide reduction electrocatalysis. Nat. Catal. *5*, 1169–1179. https://doi.org/10.1038/s41929-022-00891-3.
57. García de Arquer, F.P., Dinh, C.-T., Ozden, A., Wicks, J., McCallum, C., Kirmani, A.R., Nam, D.-H., Gabardo, C., Seifitokaldani, A., Wang, X., et al. (2020). CO_2 electrolysis to multicarbon products at activities greater than 1 A cm^{-2}. Science *367*, 661–666. https://doi.org/10.1126/science.aay4217.
58. Litvak, I., Anker, Y., and Cohen, H. (2018). In-Situ Measurements of Carbon Stable Isotopes Ratio in Karstic Caves by FTIR Spectroscopy. Int. J. Chem. Eng. Appl. *9*, 101–106. https://doi.org/10.18178/ijcea.2018.9.3.707.

STAR★METHODS

KEY RESOURCES TABLE

REAGENT or RESOURCE	SOURCE	IDENTIFIER
Chemicals, peptides, and recombinant proteins		
Copper (II) nitrate hydrate (99.999%)	Sigma Aldrich	CAS#13778-31-9
Sodium Borohydride	Sigma-Aldrich	CAS# 16940-66-2
Isopropyl alcohol (95%)	Sinopharm Chemical Reagent Co., Ltd.	CAS#67-63-0
Diethylene glycol	Sinopharm Chemical Reagent Co., Ltd.	CAS#111-46-6
Copper (II) sulfate pentahydrate (>98%)	Sigma Aldrich	CAS#7758-99-8
Potassium sodium tatrate	Sigma Aldrich	CAS#6381-59-5
Sodium hydroxide	Sigma Aldrich	CAS#1310-73-2
Formaldehyde (37 wt%)	Sigma Aldrich	CAS#50-00-0
PTFE membranes (PP laminated on one side, Pore size: 0.45 μm, Thickness: 200 μm)	GVS Filter Technology	NA
Hydrochloric Acid (37wt%)	Sigma-Aldrich	CAS#7647-01-0
Nafion 117 solution	Sigma Aldrich	CAS#31175-20-9
Graphite powder (<20 μm)	Sigma Aldrich	CAS#7782-42-5
Carbon paper (Freudenberg H14C9)	The Fuel Cell Store	NA
Carbon black (Vulcan XC-72R)	The Fuel Cell Store	CAS#1333-86-4
Iron (III) nitrate nonahydrate	Emsure	CAS#7782-61-8
Nickel (II) nitrate hexahydrate	Emsure	CAS# 13478-00-7
Potassium hydroxide flakes	Sigma-Aldrich	CAS#1310-58-3
Fumasep FAA anionic exchange membrane (AEM)	The Fuel Cell Store	NA
Software and algorithms		
EC-Lab or NOVA	Biologic or MetroOhm Autolab	https://www.biologic.net/supports/ https://www.metrohm-autolab.com/opencms/NOVA2.html
Agilent OpenLab	Agilent	https://www.agilent.com/en/product/software-informatics/analytical-software-suite/chromatography-data-systems/openlab-chemstation/
Origin 2022	Origin Lab	https://www.originlab.com/
Techno-economic analysis tool	Publication	https://doi.org/10.1016/j.xpro.2021.100889
Code used in this paper and the raw data reported here	Code on open-access repository (Zenodo)	https://doi.org/10.5281/zenodo.7565983

RESOURCE AVAILABILITY

Lead contact

Subsequent inquiries should be sent to and will be fulfilled by the lead contact, Dr. Magda H. Barecka (m.barecka@northeastern.edu).

Materials availability

No new reagents were created in the presented research.

Data and code availability

- Raw data underlying the experiments reported in this article is available (free of charge) on Zenodo. The DOI is listed in the key resources table.

- All original code is available at Zenodo, free of charge, as of the date of publication. DOIs are listed in the key resources table.
- Any additional information required to reanalyze the data reported in this paper is available from the lead contact upon request.

METHOD DETAILS

Synthesis materials

Copper (II) nitrate hydrate (99.999%) and Sodium Borohydride used for Copper nanoparticle synthesis, silver-copper alloy nanopowder (<100 nm, 98% Ag, 2% Cu), graphite powder (<20 μm) and Nafion 117 solution for GDE fabrication, and potassium hydroxide flakes used as electrolyte were acquired from Sigma Aldrich. Diethylene glycol used in Copper nanoparticle synthesis and isopropyl alcohol used in GDE fabrication inks and purification of Copper nanoparticles were used as acquired from Sinopharm Chemical Reagent Co.,Ltd. The Fumasep FAA anionic exchange membrane (AEM) were utilized to partition cathode and anode chambers of the cell, carbon black (Vulcan XC-72R) and carbon paper (Freudenberg H14C9) were used for GDE fabrication. Anode fabrication reagents Iron (III) nitrate nonahydrate and nickel (II) nitrate hexahydrate crystals were used as obtained from Emsure.

Copper nanoparticles synthesis

A 0.069493 M solution of Copper (II) Nitrate Hydrate in Diethylene Glycol was prepared in a beaker. The Copper (II) Nitrate solution was bubbled with N_2 gas for 30 minutes. 20 mL of 0.62037 M aqueous Sodium Borohydride solution was added dropwise to 140 mL of the Copper (II) Nitrate solution in a 250 mL beaker with continuous stirring at 25°C with N_2 gas bubbling. Upon complete addition of reducing agent, the reaction mixture was left to stir for 20 minutes. Purification of Copper nanoparticles were done via centrifugation at 10 000 rpm for 5 minutes with first, DI water followed by isopropyl alcohol three times. Obtained Copper Nanoparticles were vacuum dried overnight.

Copper gas diffusion electrode fabrication

Copper and Silver GDEs were fabricated via methods adapted from the procedure published by Garcia de Arquer et al.[57] The GDE consisted of 3 layers in the following sequence from bottom-up – Catalyst Nanoparticles, Carbon Black and Graphite. Each layer was hand sprayed onto 7 x 7 cm^2 carbon paper on a hot plate at 95°C with 3.2 mL of ink with the following composition – 150 mg Copper nanoparticles/ 100 mg Carbon Black/ 100 mg Graphite, 6.5 mL isopropyl alcohol, 3.5 mL DI water and 500 μL Nafion. The inks were sonicated in a 25°C water bath for 1 hour until a homogenous suspension was obtained prior to GDE fabrication.

Silver gas diffusion electrode fabrication

Silver GDEs were fabricated similarly to the Copper GDEs except for using 50 mg of Silver nanopowder instead of 150 mg in the catalyst ink.

NiFe-OOH anode fabrication (electrodeposition)

An electrodeposition solution of 3 mM aqueous solution Iron (III) Nitrate nonahydrate and 3 mM Nickel (II) Nitrate Hexahydrate was prepared. The electrodeposition was done using chronoamperometry with the set up: Working Electrode: Nickel Foam (30 x 30 mm fully immersed in electrodeposition solution), Counter Electrode: Graphite, Reference Electrode: Mercury Oxide. A voltage of -1 V was applied to the working electrode for 10 minutes. The fabricated NiFe-OOH was thoroughly rinsed with DI water and left to dry.

CO2R flow cell and electrochemical measurements

Electrochemical measurements were run using a Metroohm Autolab PGSTAT302N potentiostat. A typical 3-electrode flow cell set up were as follows – Cathode: Copper or Silver GDE, Reference Electrode: Mercury Oxide, Anode: NiFe-OOH on Ni foam. The AEM, anode and cathodes were slotted in between PTFE gaskets and plates where the AEM was slotted in between the cathode and anode. 20 mL of 3.5 KOH catholyte and 20 mL of anolyte were circulated with peristaltic pumps through the cell at a constant rate of 10 mL/min. For all flow cell characterizations, a constant CO_2 flow of 50 sccm was supplied to the flow cell. Diagnostic linear sweep voltammetry was conducted for potential range 0 to -2 V vs Hg/HgO with a scan rate of -0.05 V/s. To obtain resistance of the flow cell, a frequency response analysis (FRA) was conducted for the frequency range 0.1 to 100 000 Hz with 10 frequencies per decade.

CO2R was then performed for 9 different conditions (Table S1) under galvanostatic conditions with a run time of 10 minutes each, using Copper and Silver GDEs. The experiments were run in 2 distinct ways – 1. A 30 minutes run on the same GDE and catholyte at a constant CO_2 flow rate while increasing applied current density (conditions 1-3), 2. A 30 minutes run on the same GDE and catholyte at a constant applied current density while decreasing CO_2 flow rate (conditions 9, 6 and 3).

Analytical methods: Gas chromatography

The gaseous products from the flow cell were directly sampled into a 1 mL sampling loop of an Agilent 7890 Gas Chromatograph (GC). The products were separated with packed column Hayesep D. The GC utilized thermal conductivity detector (TCD) for hydrogen and flame ionization detector (FID) for hydrocarbon analysis. Prior to FID detection, carbon dioxide and carbon monoxide were passed through the methanizer catalyst.

NMR

For sample preparation, 10 μL of 100 mM DMSO was dropped into 1 mL of used KOH catholyte and mixed well. The mixture was put into an NMR tube. The DMSO and KOH mixture was then analyzed with magritek Spinsolve 60 Ultra NMR for liquid products analysis.

Mass spectrometry

Gaseous products from the outlet of the electrochemical flow-cell were split where 10 sccm of it sampled into a Hiden analytical QGA mass-spectrometer (UK) to on-line monitor changes in $^{12}CO_2$ and $^{13}CO_2$ concentrations during CO2R.

PTR-TOF-MS

Proton transfer reaction time-of-flight mass spectrometry (PTR-TOF-MS) was used to detect reaction products and CO_2 from the outlet flow. Modern PTR-TOF-MS instruments have high sensitivity >500 ncps/ppvb and resolution of 6000 Δm/m, allowing to trace even minor isotope enrichment effects. While the direct measurement of CO2 and CO in the PTR-TOF-MS is limited because proton affinities are 540.5 and 426.3 kJ/mol, making direct protonation from H3O+ ions impossible, the large excess of CO2 produces some amounts of carbonic acid H2CO3 in the PTR-MS drift tube. Carbonic acid has a proton affinity of 741 kJ/mol higher than for H2O (691 kJ/mol), such that it can be protonated and then detected as the H3CO3+ ion at 63.080 m/z.

A PTR-TOF-MS Qi8000 from IONICON Inc (Austria) with multiple supply reactive ions tube was utilized where H_3O^+ ions were used to ionize outgassing species. The drift tube settings were found to be optimal at 114 Td to achieve good sensitivity and resolution. The flow cell outlet was split and 1.5 sccm of it was mixed with pure nitrogen and directed into PTR-TOF-MS. Isotope contents was evaluated based on $C_2H_7O+/^{13}CCH_7O+$ ions for ethanol, $C_3H_7+/^{13}CC_2H_7+$ ions for propene and $H_3CO_3+/H_3{}^{13}CO_3+$ ions for CO_2.

Raw data from PTRMS is given in files "ag5 30 and 50 sccm.txt" and "ag 75 sccm.txt" ", for the following experiment for experiments on silver GDE with 30, 50 and 75 sccm inlet flow and 0, -0.5, -1.0, -1.5 A cm^{-2} current densities. The data was calculated using the notebook "PTR-MS and FTIR for 13C in CO2 on Ag-GDE v1.0.ipynb". Raw data and pumping effect estimated using the notebook "CO2 13C content PTR-MS v2.0.ipynb". All files are available on Zenodo https://doi.org/10.5281/zenodo.7565983.

PTR-TOF-MS background signal estimation

We estimated the background for ^{12}C and ^{13}C by measuring signals of $H_3CO_3+/H_3{}^{13}CO_3+$ ions for compressed dry air and found it as 1.8 cps and 1.6 cps respectively. Such a values may affect final isotope estimation when counts for ^{13}C are below 50 cps while for ^{12}C we might omit it as usual counts are 10^3 cps. The reason for such a background might be due to some artefacts from the ion O_4^+ that forms in the dry air because of combination of O_2^+ impurity with O_2. However, it needs to be pointed that our cell experiments include humidified CO_2 where humidity suppresses formation of O_2^+ and respectively O_4^+. To demonstrate it we performed some experiments with humidified air.

The experiment with humidified air shown that counts for ^{12}C and ^{13}C are 4.9 cps and 0.37 cps respectively. This proves our discussion above. Higher value for ^{12}C can be explained by better formation of $H_3CO_3^+$ ions in the humid atmosphere with the CO_2 in the humid air. With such a low noise we might assume that we can omit it in the future calculations as counts for $H_3{}^{13}CO_3+$ higher than 20 cps for the most cases.

Detailed calculations can be obtained from the notebook "CO2 13C content PTR-MS v2.0.ipynb".

FTIR

Fourier Transform Infrared (FT-IR) spectrometry was used to determine $^{13}CO_2$ content as an additional and independent method to confirm MS measurements. A Bruker Vertex 70 equipped with multipass gas cell and LN-MCT detector. FT-IR/PTR-TOF-MS setup is represented in Figure S3. All measurements were recorded from 2500 to 2000 cm-1wavenumber region with a scan step 1 cm-1. Before measurements were started IR gas cell was flushed with pure N2 and background noise were recorded. The flow-cell outlet was split into two streams where 5 sccm was directed to FT-IR and the rest to PTR-TOF-MS both gas streams were diluted with pure N2 to prevent detectors saturation and for faster flushing of IR gas cell, the dilution flows were 100 sccm and 200 sccm respectively. Calculation of 13C content was done by measuring intensities of the 12CO2 P-branch absorption at ν = 2343 cm-1 and the P-branch of the $^{13}CO_2$ absorption at ν = 2273 cm^{-1}. Then the ratio of two peaks were assessed to obtain the change of $^{13}CO_2$ content.[58] Exemplary FTIR spectra are given in the Figure S7.

Flow cell characterization and products

A linear sweep voltammetry (LSV) was performed on the flow cell to obtain the current-voltage behavior of each GDE (Figures S1A and S2A). Electrochemical impedance spectroscopy (EIS) was then conducted to obtain a frequency response analyzer (FRA) plot to determine the cell's resistance (Copper GDE flow cell: 0.99 Ω, Silver GDE Flow cell: 1.10 Ω) (Figures S1B and S2B).

All CO_2R was conducted via chronopotentiometry (CP). The Figures S1 and S2 present a typical LSV, FRA and CP for copper and silver GDEs respectively.

Faradaic efficiency calculations

Gaseous Products Liquid Products

$$FE\ (\%) = \frac{x.F.V.p.v}{R.T.I} \times 100\% \quad FE\ (\%) = \frac{x.F.n}{I.t} \times 100\%$$

Where,***x*** = number of electrons required for hydrogenation of CO_2 to form a specific productGas products: x for H_2 = 2e^-, CO = 2 e^-, CH_4 = 8 e^-, C_2H_4 = 12 e^-Liquid products: x for HCOOH = 2 e^-, CH_3COOH = 8 e^-, C_2H_5OH = 12 e^-F = 96 485 C/molV (m3/s) = Gas flow rate recorded at the exhaust of the flow cell using a flow meter under room temperature and ambient pressure.p = 1.01 X 105 Pav (Vol%) = Volume concentration of product in exhaust gas of the cell (GC data)R = 8.314 Nm/mol KT = 298.15 KI (A) = Current applied to flow celln (mol) = Moles of liquid product (Calculated from concentration of liquid product in electrolyte determined by NMR analysis)t (s) = Duration of CO2R

To covert the product flow (mol/cm^2 s) into the total product flow (mol/s), we multiplied the product flow by the active surface of the electrode (surface exposed to both gas and catholyte), being approximately 1 cm^2.

Process modelling

We sought to conceptually design a complete process to manufacture ^{13}C enriched streams by means of CO_2 electrolysis (Figure 3B), targeting 5 vol% ^{13}C content in CO_2 stream. To this end, we will deploy a series of consecutive electrolyzers assuming a feasible CO_2 conversion at each step. As the remaining stream of CO_2 after the first electrolyzer will decrease (due to conversion of CO_2 to CO), the second electrolyzer will be proportionally smaller in size. The extent of ^{13}C enrichment during the electrochemical reaction is extrapolated from the experimentally derived relationship between products flow rate and $\Delta^{13}C$ for the best enrichment conditions. We used a process modelling protocol published by Barecka et al.[53] to assess the composition of the streams leaving the electrolysis reactor, as well as energy and water consumption. Following data was used as the input to the calculation tool attached to the protocol:

- 50% conversion of CO_2 in one stage (assumed as a realistic forward-looking target based on available reports on electrolyzers scale-up[49])
- Current density: 1.5 A/cm^2 (as determined during experiments[45])
- Full cell voltage: 3 V (voltage reported for the most stable for electrolyzers tested for long-time operation[45])
- Faradaic efficiency: 30% for CO (as determined during experiments)

Modelling results, computed from the tool attached to the protocol by Barecka et al.[3] are summarized in Table S8. We envision different options for separation of CO_2 from the gas stream leaving the electrolyzer, e.g. low temperature phase separation[52] or membrane-based processes.[51] Following process evaluation includes the most mature option; separation by means of distillation, flash separation, internal heat recovery and auxiliary refrigeration. We assessed the energy input for this separation by based on detailed modelling and resulting the energy requirement for a process with a similar composition of stream on the inlet and outlet of the separation section; details are given in publication by Berstad et al.[52]

- Energy requirement for separation: 0.36 MJ/kg of CO_2

Techno-economic analysis

To assess manufacturing costs, we used described above process model and considered the following cost indicators:

- 0.05 $/kWh of renewable energy powering the process (relatively high cost based most recent reports on renewable energy prices[54])
- 200$/kg of CO_2 (CO_2 costs for direct air CO_2 capture,[55] being the most expensive source of biogenic CO_2).

Lastly, energy requirement for electrolysis and separation are summed up and multiplied by the energy cost. Total cost of ^{13}C production by electrolysis was assessed as (Equation 6):

$$C13\ enriched\ CO_2\ production\ cost\ = \frac{total\ electricity\ cost + water\ costs + CO_2\ cost\ \left(\frac{\$}{s}\right)}{outlet\ flowrate\ of\ enriched\ CO_2\ \left(\frac{\$}{s}\right)} \quad \text{(Equation 6)}$$

While CO_2 electrolysis will deliver also a significant flow rate of syngas and oxygen products, we did not consider any economic benefit from selling these products.

The cost of commercially available 5% ^{13}C enriched CO_2 was extrapolated from the price[48] of 99% ^{13}C enriched CO_2 by multiplying the latter by 5%. This assessment might lead to actual underestimation of the price of commercially available ^{13}C and the actual price might be a higher. However, more detailed price assessments are currently not available.